

1
2 **Main Manuscript for**

3 **Regional Variation in the Role of Humidity on City-level Heat-Related**
4 **Mortality**

5 **Qiang Guo^{1,2*}, Malcolm N. Mistry^{3,4}, Xudong Zhou^{2,5}, Gang Zhao², Kanon Kino¹, Bo Wen⁶, Kei Yoshimura²,**
6 **Yusuke Satoh⁷, Ivana Cvijanovic⁸, Yoonhee Kim⁹, Chris Fook Sheng Ng¹⁰, Ana M. Vicedo-Cabrera^{11,12}, Ben**
7 **Armstrong¹³, Aleš Urban^{14,15}, Klea Katsouyanni^{16,17}, Pierre Masselot³, Shilu Tong^{18, 19, 20}, Francesco Sera²¹,**
8 **Veronika Huber^{22,23}, Michelle L. Bell^{24,25}, Jan Kyselý^{14,15}, Multi-Country Multi-City (MCC) Collaborative**
9 **Research Network[#], Antonio Gasparrini³, Masahiro Hashizume¹⁰, Taikan Oki¹**

10 ¹ Department of Civil Engineering, Graduate School of Engineering, The University of Tokyo, Tokyo, 113-0033,
11 Japan

12 ² Institute of Industrial Science, The University of Tokyo, Tokyo, 153-8505, Japan

13 ³ Environment & Health Modelling (EHM) Lab, Department of Public Health, Environments and Society, London
14 School of Hygiene & Tropical Medicine, London, UK

15 ⁴ Department of Economics, Ca' Foscari University of Venice, Venice, Italy

16 ⁵ Institute of Hydraulics and Ocean Engineering, Ningbo University, Ningbo 315211, China

17 ⁶ Climate, Air Quality Research (CARE) Unit, School of Public Health and Preventive Medicine, Monash University,
18 Level 2, 553 St Kilda Road, Melbourne, VIC 3004, Australia

19 ⁷ Moon Soul Graduate School of Future Strategy, Korea Advanced Institute of Science and Technology, Daejeon,
20 Republic of Korea

21 ⁸ Barcelona Institute for Global Health - ISGLOBAL, Doctor Aiguader 88, 08003 Barcelona, Spain

22 ⁹ Department of Global Environmental Health, Graduate School of Medicine, The University of Tokyo, Tokyo 113-
23 0033, Japan

24 ¹⁰ Department of Global Health Policy, Graduate School of Medicine, The University of Tokyo, Tokyo 113-0033,
25 Japan

26 ¹¹ Institute of Social and Preventive Medicine, University of Bern, Bern, Switzerland

27 ¹² Oeschger Center for Climate Change Research, University of Bern, Bern, Switzerland

28 ¹³ Department of Public Health, Environments and Society, London School of Hygiene & Tropical Medicine, London,
29 United Kingdom

30 ¹⁴ Institute of Atmospheric Physics, Czech Academy of Sciences, Prague, Czech Republic

31 ¹⁵ Faculty of Environmental Sciences, Czech University of Life Sciences, Prague, Czech Republic.

32 ¹⁶ Department of Hygiene, Epidemiology and Medical Statistics, National and Kapodistrian University of Athens,
33 Greece

34 ¹⁷ Environmental Research Group, School of Public Health, Imperial College London, London, UK

35 ¹⁸ School of Public Health and Social Work, Queensland University of Technology, Brisbane, Australia

36 ¹⁹ School of Public Health and Institute of Environment and Human Health, Anhui Medical University, Hefei, China

37 ²⁰ Shanghai Children's Medical Centre, Shanghai Jiao-Tong University, Shanghai, China

38 ²¹ Department of Statistics, Computer Science and Applications "G. Parenti", University of Florence, Florence, Italy

39 ²² Chair of Epidemiology, Institute for Medical Information Processing, Biometry, and Epidemiology (IBE), Faculty
40 of Medicine, LMU Munich, Munich, Germany

41 ²³ Institute of Epidemiology, Helmholtz Zentrum München – German Research Center for Environmental Health,
42 Neuherberg, Germany

© The Author(s) 2024. Published by Oxford University Press on behalf of National Academy of Sciences. This is an Open Access article distributed under the terms of the Creative Commons Attribution-NonCommercial License (<https://creativecommons.org/licenses/by-nc/4.0/>), which permits non-commercial re-use, distribution, and reproduction in any medium, provided the original work is properly cited. For commercial re-use, please contact reprints@oup.com for reprints and translation rights for reprints. All other permissions can be obtained through our RightsLink service via the Permissions link on the article page on our site—for further information please contact journals.permissions@oup.com. 1

1 ²⁴ School of the Environment, Yale University, New Haven CT, USA

2 ²⁵ School of Health Policy and Management, College of Health Sciences, Korea University, Seoul 02841, Republic
3 of Korea

4
5 *Corresponding author, E-mail: qiang@rainbow.iis.u-tokyo.ac.jp

6
7 # A full list of authors from the Multi-Country Multi-City (MCC) Collaborative Research
8 Network is in the Acknowledgements

9
10 **Author contributions:** Q.G. and T.O. conceived and designed the study. Q.G. conducted the calculation and
11 analysis. M.H. and M.N.M. managed the mortality data. X.Z., K.K., K.Y., Y.S., M.N.M., and I.C. contributed to the
12 climatological analysis. M.N.M., A.G., and B.W. contributed to the DLNM analysis. G.Z. contributed to the
13 machine learning analysis. Q.G. drafted the manuscript. All authors edited the manuscript.

14
15 **Competing Interest Statement:** The authors declare no competing interests.

16 **Classification:**

17 Major: Biological, Health, and Medical Sciences

18 Minor: Public Health and Epidemiology

19
20
21 **Keywords:** Humidity, Mortality, Heat Stress, Urban Climate, Climate Change

22 **This PDF file includes:**

23 Main Text

24 Figure Captions 1 to 5

25 **Abstract**

26
27
28
29
30 The rising humid heat is regarded as a severe threat to human survivability, but the proper integration of
31 humid heat into heat-health alerts is still being explored. Using state-of-the-art epidemiological and
32 climatological datasets, we examined the association between multiple heat stress indicators (HSIs) and
33 daily human mortality in 739 cities worldwide. Notable differences were observed in the long-term trends
34 and timing of heat events detected by HSIs. Air temperature (T_{air}) predicts heat-related mortality well in
35 cities with a robust negative T_{air} -relative humidity correlation ($C_{T\text{-RH}}$). However, in cities with near-zero
36 or weak-positive $C_{T\text{-RH}}$, HSIs considering humidity provide enhanced predictive power compared to T_{air} .
37 Furthermore, the magnitude and timing of heat-related mortality measured by HSIs could differ largely
38 from those associated with T_{air} in many cities. Our findings provide important insights into specific regions
39 where humans are vulnerable to humid heat and can facilitate the further enhancement of heat-health alert
40 systems.

41 **Significance Statement**

42
43 Climate change has intensified the frequency, duration, and severity of lethal heat stress in recent years, a
44 trend expected to exacerbate further. Despite the increasing focus on humid heat, there remains a gap in
45 understanding how to effectively integrate humid heat into heat-health alert systems across regions with
46 diverse climatic conditions. Addressing this gap, our study utilizes extensive epidemiological and
47 climatological datasets to discern locations where incorporating humidity largely improves the predictive

1 capacity for heat-related mortality compared to relying solely on air temperature. These findings offer
2 crucial insights for enhancing heat-health alert systems in the face of ongoing climate change.

5 Introduction

6 In recent decades, global warming has led to an increase in the intensity, duration, and frequency of heat
7 waves^{1,2}, an effect that is projected to worsen in the future^{3,4}. With record-breaking heatwaves observed
8 worldwide, the 2022 and 2023 heatwaves provided a glimpse into what the future is expected to bring. In
9 2022, Tokyo recorded nine consecutive days of temperatures above 35 °C, marking the most severe
10 heatwave since official temperature records began in the 1870s. In the United Kingdom, for the first time,
11 the temperature reached 40 °C⁵. More recently, parts of Spain broke high-temperature records for April in
12 the spring heatwave of 2023. These events highlight a major concern for human health because exposure
13 to high outdoor temperatures can significantly increase the risk of mortality and morbidity⁶⁻⁸. For example,
14 in Europe only, heatwaves were responsible for over 120,000 reported deaths between 1970 and 2012,
15 accounting for 85% of all climate disaster-related deaths⁹, and in 2022 alone, heatwaves are estimated to
16 have resulted in over 70,000 excess deaths across Europe¹⁰.

17 The human body responds to heat stress in two primary ways to release the heat: vasodilation and
18 perspiration. Vasodilation enhances heat transfer from muscles to skin via blood flow, while perspiration
19 removes heat from the skin to the environment through sweating and evaporative cooling¹¹. Although
20 perspiration plays a crucial role in heat dissipation, its efficacy is affected by ambient humidity, wind
21 speed, and ventilation^{12,13}. As a result, human-perceived heat stress depends not only on the air temperature
22 (dry bulb, T_{air}) but also humidity, wind speed, and incident radiation. To measure the combined impact of
23 multiple climate variables on human perceived heat stress, many heat stress indicators (HSIs) have been
24 proposed, which all consider T_{air} and relative humidity (RH), some also wind speed and solar radiation¹⁴.
25 These HSIs are increasingly utilized in climate change impact studies and are viewed as a better metric
26 for quantifying the heat stress burden on human health (i.e., morbidity and mortality) than T_{air} ^{3,4,15-20}. Some
27 widely used HSIs include wet bulb temperature (T_w)²¹, wet bulb globe temperature (T_{WBG})²², heat index
28 (HI)²³, and apparent temperature (APT)²⁴.

29 Despite being widely used, several key questions about HSIs remain unclear. First, while many scholars
30 expect HSIs to perform better than T_{air} in predicting human mortality based on physiological evidence²⁵,
31 existing population-scale epidemiological studies have not provided consistent evidence to support this²⁶⁻
32 ³². Therefore, epidemiologists continue to rely on T_{air} to quantify excess deaths related to heat stress^{6,7,33}.
33 Secondly, there are over 100 proposed HSIs in the literature, each based on different principles and
34 assumptions, but there is no consensus on their proper usage or the strengths and limitations of each¹⁴.
35 Recent research indicates that the HSI that best reflects health consequences may vary by country, and the
36 estimated heat-related mortality using the optimal HSI could be similar to that of T_{air} , although apparent
37 cross-country variations are observed³². Additionally, HSIs exhibit different sensitivities to changes in T_{air}
38 and RH (Fig. S1 in the supplementary)¹², and in some cases, may even suggest opposite effects under
39 specific conditions. For example, regional climate simulations show that irrigation in northern India results

1 in a higher T_w but a lower HI¹⁶, making it challenging to measure and interpret changes in regional heat
 2 stress. To date, the role of humidity in heat-related health outcomes has become a heated discussion³⁴.
 3 However, to the best of our knowledge, no study has yet examined how to appropriately use HSIs for
 4 population-scale heat-health alerts and health impact assessments related to climate change, particularly
 5 in regions characterized by diverse climate conditions.

6 Here, we conduct a detailed investigation on the association between multiple HSIs and human mortality
 7 at the city level, using state-of-the-art climatological (ERA5 reanalysis³⁵) and epidemiological data (Multi-
 8 Country Multi-City (MCC) database, <https://mccstudy.lshtm.ac.uk/>, see Materials and Methods) for 1980-
 9 2019. The analysis incorporates multiple widely used and contrasting HSIs calculated at hourly timescales,
 10 and covers 739 cities^a from 43 countries and territories (Fig. S2, Tables S1 and S2) spanning different
 11 climate regimes. Specifically, we examined the long-term trend and timing of heat stress events for
 12 multiple HSIs, and assessed their advantages in modelling/predicting city-level human mortality in lieu of
 13 T_{air} , as well as the spatial heterogeneity in their performances. Importantly, we identify the specific regions
 14 where humidity has a discernible impact on heat-related mortality and describe their common
 15 climatological features using machine learning, a crucial research question not known to have been
 16 addressed in studies to date. The findings of this study provide essential information for facilitating high-
 17 accuracy heat-health alert systems, which can provide enhanced protection from heat under future climate
 18 change.

19 Results

20 Discrepancy among heat stress indicators

21 We investigated trends in extreme temperatures and six different HSIs (T_w ²¹, simplified wet bulb globe
 22 temperature (T_{sWBG})³⁶, Humidex (H_x)³⁷, APT²⁴, Universal Thermal Climate Index (UTCI)³⁸, and HI²³, see
 23 Materials and Methods, and Table S3) from 1980 to 2019 (Fig. 1). Specifically, we calculated the 99th
 24 percentile of daily near-surface air temperature T_{air} (X_{99}) for each year and estimated its average decadal
 25 change (Fig. 1a). We then similarly examined the trends in near-surface specific humidity (Q) and relative
 26 humidity (RH) for high-temperature days ($T_{air} > X_{99}$) of each year (Fig. 1b, c).

27 To quantify the discrepancy in trends over time among the six HSIs, we introduced the HSI vote. This
 28 measures the agreement of the trend direction among the X_{99} of HSIs, with a vote of 1 assigned for a
 29 positive trend and -1 for a negative trend. We then summed the HSI votes (possible values: -6, -4, -2, 0,
 30 2, 4, 6) for each region to show the overall trend agreement (Fig. 1d, e). Our analysis shows that T_{air} X_{99}
 31 exhibits positive trends over most regions due to global warming, while a limited number of regions show
 32 no increase or a slight decrease (e.g., Midwest US, Canada, Central Asia, and northern Australia, Fig. 1a)
 33 potentially due to factors such as irrigation³⁹. Both positive and negative trends are observed for Q of high-
 34 temperature days, while a larger proportion of the land surface shows negative trends for RH (Fig. 1b, c).
 35 The reduction in near-surface RH can be attributed to several factors. It may result from the constrained
 36 addition of water vapor to the air as the saturation vapor pressure increases^{40,41}. Additionally, variations
 37 in warming rates between land and ocean surfaces can also contribute to the observed decrease in near-

^a In the MCC dataset, the daily mortality is collected on a region/prefecture basis for some countries (i.e., Ireland, Japan, and Czech Republic).

1 surface RH over land. These diverging trends of T_{air} extremes and their RH result in discrepancies in the
2 long-term trends of the HSIs as they have different sensitivities to changes in T_{air} and RH (Fig. S1).

3 Our analysis reveals severe contrasting trends among HSIs in Midwest US, Canada, South Africa, Central
4 Asia, and Australia (HSI vote sum=0, yellow colour in Fig. 1d, e). These contradictions are more
5 significant for results based on the daily maximum value of HSI (Fig. 1e). This finding reveals the potential
6 of providing misleading or contradictory information when quantifying regional heat stress changes based
7 on a single HSI^{3,4,15,18,19}.

8 We also examined the discrepancy in the intra-annual peak time (PT, the day of the year when a given
9 indicator reaches its highest annual value) for HSIs and T_{air} (Fig. 2a-g). T_{air} typically peaks in February-
10 April in tropical regions, and in June-August and December-March for northern and southern extratropical
11 regions, respectively (Fig. 2a). We found appreciable differences between the PTs of HSIs and T_{air} ,
12 particularly in northern tropical regions where the PT of HSIs (Fig. 2b-g) occurs much later than that of
13 T_{air} , and in the southern tropical regions, where the PT of HSIs occurs much earlier. HSI peak times are
14 clearly modulated by the position of tropical rainfall belts and the seasonal movement of summer
15 monsoons. However, for the extratropical regions, only slight differences are observed. The PT
16 discrepancy with T_{air} also varies among HSIs, with those more sensitive to RH (i.e., T_w and T_{sWBG} , Fig.
17 2b, c, Fig. S1) showing larger PT discrepancies than those less sensitive to RH (i.e., UHCI and HI, Fig. 2f,
18 g).

19 We further examined the PT discrepancy in four MCC cities (Austin, Brasilia, London, and Bangkok)
20 located in different regions using T_{air} and eight HSIs (see Materials and Methods), focusing on the
21 occurrence frequency of the hottest ten days (Fig. 2h-k). In Austin and Brasilia, there were apparent timing
22 differences for HSIs, particularly T_w , compared to T_{air} . In contrast, London and Bangkok had relatively
23 small discrepancies. These variations can be attributed to the cities' distinct climatic characteristics (Fig.
24 S3). RH was less influenced by changes in T_{air} in London and Bangkok and maintained consistently high
25 values throughout the year (Fig. S3c, d). Conversely, Austin and Brasilia experienced significant
26 reductions in RH during the summer when T_{air} increased (Fig. S3a, b), leading to a limitation in the
27 increase of T_w and resulting in discrepancies in PT with T_{air} . The low overlap rate in some regions between
28 the annual hottest 10 and 30 days of HSIs and T_{air} further emphasizes the challenge of early warning for
29 heat stress when using different HSIs and T_{air} (Fig. S4). This analysis highlights the need for improved
30 understanding and applying appropriate HSIs (as well as T_{air}) in heat stress forecasting.

31 **Spatial diversity of the best-fit indicators to city-level mortality**

32 To investigate which indicator, either T_{air} or multiple HSIs, provides better predictive power for modelling
33 city-level mortality across 739 MCC cities, we evaluated the association between the daily mean value of
34 these indicators and daily mortality during the warm season (defined as the six warmest consecutive
35 months in each city, provided in Table S2). We then used the quasi-Akaike information criterion (qAIC)⁴²
36 to evaluate the goodness of fit of the models (see Materials and Methods). The best-fit indicator (BFI) was
37 defined as the indicator with the lowest qAIC.

38 Our analysis reveals that the BFI varies for cities in different regions (Fig. 3). Fig. 3a presents the BFIs
39 with a focus on their sensitivity to RH. The result suggests that humid heat may play a more important
40 role in influencing human mortality in coastal and large lake areas of the U.S., Peru, Thailand, Korea, and

1 Japan, where the BFI tends to have a high sensitivity to RH. However, for other regions, such as
 2 Argentina, Portugal, southern Spain, and South Africa, dry heat (without or with slight consideration of
 3 RH) is more closely associated with human mortality. Overall, T_{air} demonstrates the highest performance
 4 among all indicators for approximately 30% (222 out of 739) of MCC cities (Fig. 3b). However, HSIs also
 5 exhibit strong performance in the other 517 cities. The qAIC differences between T_{air} and the BFI for the
 6 517 cities (Fig. S5) are large enough to make chance an unlikely explanation for their better fit (averaged
 7 qAIC differences > 2)⁴³.

8 As our objective is to examine the performance of these HSIs compared to T_{air} , we investigate the number
 9 of HSIs that surpass T_{air} 's performance for each city (Fig. S6). The result indicates that for the cities whose
 10 BFI has high humidity sensitivity, the use of other indicators considering humidity even marginally in
 11 their formulation also exhibits superior performance to T_{air} in general (compare Fig. 3a and Fig. S6a).

12 In addition, using the daily maximum indicator values and quasi-Bayesian information criterion (qBIC)⁴²,
 13 we obtained similar spatial patterns of BFIs (Figs. S7 and S8), strengthening the robustness of our findings.
 14 In most cities, the daily mean value of the indicators slightly outperformed the daily maximum value in
 15 modelling city-level mortality, except for Central America (Fig. S9). Detailed information on the qAIC of
 16 each indicator and the BFI of 739 cities can be found in Table S4.

17 **Under what conditions does humid heat matter more for mortality**

18 To gain insights into why humid heat stress has a higher association with human mortality in certain
 19 regions and cities, we compared two groups of cities: dry heat cities with a BFI of T_{air} (222 cities) and
 20 humid heat cities with a BFI of one of the humidity sensitive HSIs: T_w , T_s , T_{WBG} , or T_{sWBG} (231 cities).
 21 The qAIC difference between HSIs and T_{air} for these groups is shown in Fig. S10. We also compared the
 22 performance of each HSI and T_{air} for all 739 cities and 231 humid heat cities in Fig. S11. The results reveal
 23 that, across all 739 cities, T_{air} generally outperforms individual HSIs, except for HI. However, in humid
 24 heat-dominant cities, most HSIs (except for UTCI) show better performance than T_{air} (Fig. S11).

25 We collected 13 features for each city, covering climatological, geographical, and socio-economic factors,
 26 and used them as inputs to train a random forest model to classify the cities into the two groups (see
 27 Materials and Methods, and Tables S5 and S6). Our supervised machine learning model was able to
 28 distinguish between the two groups of cities, with accuracy, precision, and recall of 65.6%, 66.3%, and
 29 65.5%, respectively (see the confusion matrix in Table S7). We identified the top two factors that
 30 influenced the classification to be the correlation between daily T_{air} and RH during the warm season ($C_{T_{\text{air}}}$
 31 $_{\text{RH}}$) and latitude (Fig. 4a).

32 The $C_{T_{\text{air}}}$ $_{\text{RH}}$ emerges as the most important factor in determining the influence of humidity on heat-related
 33 mortality at the city level. $C_{T_{\text{air}}}$ $_{\text{RH}}$ is negative in many cities (Fig. 4b), indicating that as T_{air} rises, the air can
 34 hold more water, but the local environment fails to provide sufficient water vapor, resulting in decreased
 35 RH⁴¹. This phenomenon can be observed in the time series of T_{air} and RH of Austin and Brasilia (Fig. S3a,
 36 b). However, we also found that some cities (many of them coastal) have positive $C_{T_{\text{air}}}$ $_{\text{RH}}$ (Fig. 4b), although
 37 this correlation is usually weak. In Fig. 4c, we plot the BFI against $C_{T_{\text{air}}}$ $_{\text{RH}}$ for the 739 MCC cities. Dry heat
 38 cities with RH-insensitive BFIs (e.g., T_{air}) exhibit clear negative $C_{T_{\text{air}}}$ $_{\text{RH}}$, while cities with RH-sensitive
 39 BFIs (e.g., T_w , T_s , T_{WBG}) predominantly display near-zero or weak positive $C_{T_{\text{air}}}$ $_{\text{RH}}$ associations (Fig. 4c).
 40 The spatial distribution also suggests that there is a significant overlap between the locations of cities with

1 moderate positive C_{T-RH} and where humidity is influential to heat-related mortality (compare Fig. 4b and
 2 Fig. 3a). Substituting RH with specific humidity (Q) as input features, we obtained comparable results for
 3 the feature importance. These findings underscore the importance of the temperature-humidity correlation
 4 in determining the health impacts of humid heat.

5 Furthermore, another result also suggests that the relative performance of HSIs tends to increase as C_{T-RH}
 6 transitions from strongly negative to moderately positive. We analysed the qAIC difference between each
 7 HSI and T_{air} in relation to the C_{T-RH} of cities (Fig. S13). With a higher positive C_{T-RH} , T_{air} 's performance
 8 declines, whereas HSIs (except for UTCI) show clear improvement, although C_{T-RH} alone cannot perfectly
 9 separate the data points by $\Delta qAIC=0$ as it is influenced by factors such as latitude. Notably, for cities with
 10 $C_{T-RH} > 0$, HSIs such as HI, T_{WBG} , and T_S exhibit better performance than T_{air} (Fig. S13a, f, g). The same
 11 analysis using the daily maximum value of indicators, which is more frequently used in issuing a heat
 12 alert, shows a more apparent trend, which further demonstrates the robustness of the findings (Fig. S14).

13 Our general interpretations of the results are as follows: Firstly, in cities with a strong negative C_{T-RH} , the
 14 daily variation in RH is already captured by T_{air} change due to their strong negative correlation. Therefore,
 15 using HSIs that place excessive emphasis on humidity (e.g., T_w , which assumes the human body is naked
 16 and fully wet) does not yield improved predictive performance. In these cities, T_{air} emerges as the superior
 17 predictor. However, in cities with a relatively weak C_{T-RH} , explicitly considering the variation in RH
 18 becomes necessary, and HSIs that account for humidity provide improved predictive power compared to
 19 T_{air} alone. Secondly, in cities with a strong negative C_{T-RH} , the occurrence of simultaneously high T_{air} and
 20 high RH is unlikely due to their mutual constraint. However, in cities with a near-zero or positive C_{T-RH} ,
 21 the likelihood of such co-occurrence increases, resulting in a higher risk of severe humid heat stress that
 22 significantly impacts human mortality.

23 **Heat-related mortality estimation using air temperature and the best-fit heat stress indicator**

24 To estimate heat-related deaths, we applied location-specific exposure-response functions to the warm-
 25 season T_{air} and the BFI time series (see Materials and Methods). We calculated the attributable fraction
 26 (AF, %) of heat-related mortality as the number of deaths attributed to heat divided by the total number of
 27 deaths during the warm season, for the 517 cities whose BFI is one of HSIs (see Materials and Methods).
 28 We also analysed the exposure-response curves and the intra-annual variation of the mortality relative risk
 29 (RR) averaged between 1980-2019 for four big cities (Miami, Bristol, Ho Chi Minh City, and Taipei)
 30 located in different regions (Fig. 5).

31 The RR increases significantly when T_{air} and the BFI exceed the optimum values for all four cities (Fig.
 32 5a, c, e, g). Bristol and Ho Chi Minh City had shorter heat stress exposure periods when estimated using
 33 BFI compared to T_{air} (Fig. 5d, f), and smaller BFI-estimated heat-related AFs of 0.39% (95% CI
 34 (Confidence Interval): -0.21 – 0.93) and 2.50% (95% CI: 0.91 – 3.97), respectively, compared to T_{air} -
 35 estimated AFs of 0.42% (95% CI: -0.94 – 1.68) and 2.67% (95% CI: 0.01 – 5.11). In particular, the timing
 36 of the highest RR notably differs between T_{air} and the BFI (specifically T_{WBG}) at Ho Chi Minh City,
 37 providing distinct information relevant to an effective heat stress early warning system. On the other hand,
 38 BFI-estimated mortalities were higher than T_{air} -estimated for Miami and Taipei, with a similar heat stress
 39 exposure period between T_{air} and the BFI (Fig. 5b, h). These findings demonstrate that the choice of HSI
 40 can be critical for the estimation of both the total number and timing of heat stress-related deaths.

1 The warm-season heat-related AF estimated by T_{air} averaged 2.25% (95 % CI: -1.61 – 5.11) across these
2 517 cities, with higher mortality in cities in Europe, Peru, Southeast Asia, and some regions in the US
3 (Fig. S15a, b). The BFI estimated a slightly higher AF of 2.39% (95% CI: -1.55 – 5.14) during the warm
4 season compared to T_{air} . The AF difference varied across cities, with relatively small variations in the
5 Midwest US and Japan, but larger deviations among cities in Peru, Europe, and Southeast Asia, indicating
6 a large divergence from T_{air} estimates (Fig. S15c, d). However, it is important to interpret these specific
7 mortality numbers and differences with caution, as AFs do not measure predictive performance, and they
8 may be influenced by data length, quality, and other factors, introducing potential uncertainties (Fig. S16).

9 Discussion

10 In this study, we analysed state-of-the-art epidemiological and climatological data to examine the
11 influence of humidity on heat-related mortality at the city level. Our findings indicate that for the majority
12 of the cities examined that feature a robust negative T_{air} -RH correlation, the commonly used temperature
13 indicator T_{air} could be a reasonable predictor, and properly incorporating the low-weight humidity term
14 (i.e. HI) only moderately improves the predictive power. However, T_{air} 's performance in predicting
15 mortality tends to decline when C_{T-RH} is near-zero or weakly positive (i.e., coastal and large lake areas of
16 the US, Peru, Korea, and Japan), while HSI with a higher emphasis on humidity often demonstrate
17 improved performance and can outperform T_{air} . We also quantify heat-related deaths using the BFI, which
18 reveals differences in both the number and timing of deaths compared to estimates based on T_{air} . These
19 findings provide important information for the development of city-level heat-action plans and adaptive
20 strategies through localized heat-health warning systems based on the BFI.

21 Our study encompasses 739 cities across 43 countries/territories, with a time series spanning part or all of
22 1980-2019. Additionally, to capture the simultaneity of multiple climate variables, we calculated HSIs on
23 an hourly scale. Collecting continuous time series of hourly T_{air} , RH, wind speed, and solar radiation data
24 with such temporal and spatial coverage is challenging. Thus, climate reanalysis data such as ERA5,
25 combining multi-source observations and model simulations, provides a viable alternative. To verify the
26 reliability of ERA5 in accurately representing the association between T_{air} and RH, we compared the C_{T-RH}
27 during the warm season from ERA5 to climate observations. The C_{T-RH} of ERA5 is verified with climate
28 observations for 476 out of 739 MCC cities, for which the observed daily T_{air} and RH are available in the
29 MCC dataset (Fig. S17). These observations were collected from representative weather stations in the
30 respective cities, covering part of the periods between 1980-2019, totaling more than five years for each
31 city. For the same periods, we found that the spatial pattern of C_{T-RH} from ERA5 matches well with the
32 observational data. Specifically, both datasets reveal weak positive C_{T-RH} in cities in the western US,
33 Ireland, Korea, and Japan, and strong negative C_{T-RH} in the eastern US, Brazil, southern Europe, and
34 Southeast Asia. Given the high consistency between C_{T-RH} from ERA5 and in-situ data, we believe ERA5
35 reliably represents C_{T-RH} for the cities studied.

36 Compared to urban climate studies, which focus more on investigating the spatial diversity of the urban
37 heat^{44,45}, environmental health studies emphasize temporal fluctuations of the exposure and their short-
38 term associations with city-level health outcomes. Environmental health studies typically use one
39 representative climate station per city to represent the general climate conditions and build associations
40 with population-scale health outcomes. This approach is standard in the environmental health research
41 community and has been well demonstrated by previous studies^{6,7,42}. Additionally, studies such as Mistry
42 et al. (2022)⁴⁶ have shown that ERA5 data compare well with in-situ data from representative stations in

1 environmental health analyses, with similar model fitness and temperature-related risk estimates. Guo et
2 al. (2024)⁴⁷ also validated ERA5's daily mean T_{air} and RH against observations from representative climate
3 stations for 47 prefectures in Japan, finding good consistency. Given ERA5's reliable performance, high
4 temporal and spatial resolution, and global coverage, it has become widely demonstrated and used in
5 environmental health studies^{32,48,49}.

6 Nonetheless, some limitations to our study should be discussed. Although we analysed data from over 700
7 cities worldwide, the majority of these cities are located in developed countries, constraining us from
8 conducting analysis for other regions facing severe humid heat stress, such as the Persian Gulf, northern
9 India, and North China Plain⁵⁰, due to data scarcity. Additionally, our machine learning model utilized
10 thirteen city features as inputs, achieving a modest accuracy of 65.6%. However, possibly important
11 factors, including race, air conditioning availability, and medical infrastructure were not included due to
12 data unavailability, which in turn could have limited the accuracy of the random forest model. We did not
13 evaluate the separate impact of wind speed and solar radiation, included in some HSI (UTCI, APT, and
14 TWBG), from that of RH, due to the fact that these were not particularly high-performing indicators.

15 Although previous studies have demonstrated a strong agreement between HSIs calculated from multiple
16 reanalysis datasets and those derived from station-based data^{44,46,47}, discrepancies remain when compared
17 to observations, and also among different reanalysis datasets. These discrepancies can vary by climate
18 region and meteorological variable⁴⁴. Therefore, further research and improved data gathering by
19 enhancing local weather station networks are crucial to reduce measurement errors and deepen our
20 understanding of heat stress measures and their health impacts. Additionally, we acknowledge that while
21 the feature importance analysis identified C_{T-RH} as a significant factor influencing the relative performance
22 of different HSIs, this method does not provide insights into causality. Investigating the sensitivity of
23 population-scale residents to humid heat stress involves numerous multidisciplinary factors, including
24 climatic, socio-economic, demographic, and human behavioral elements. Our study represents an initial
25 attempt to understand the spatial heterogeneity in the performance of different HSIs and the role of
26 humidity in health impacts. Further research encompassing physiological, demographic, and
27 epidemiological areas is needed to enhance our understanding of the causality involved.

28 Despite these limitations, the results presented here provide important new aspects for understanding the
29 role of humidity in the epidemiological analysis of heat-related mortality. The findings may bridge the
30 recognition gap among physiological, climatological, and epidemiological communities on the association
31 between humid heat and health outcomes, a heated debate across communities. As for further research,
32 integrating this city-level mortality analysis with individual-level heat stress adaptability experiments²⁵
33 could enhance our understanding of the health effects of humid heat stress. Given the risk of heat waves
34 globally, our results demonstrate the importance of considering humidity in heat stress prediction and
35 heat-action plans for regions with a non-negative temperature-humidity correlation.

36 **Materials and Methods**

37 **Mortality data.** We obtained daily mortality data for our study from the Multi-Country Multi-City (MCC)
38 Collaborative Research Network database (<https://mccstudy.lshtm.ac.uk/>). A summary of the data for each
39 country is provided in Table S1 in the supplementary, and the full list of cities included in our analysis is
40 provided in Table S2. We used all-cause or non-external cause deaths (ICD-9: 0-799; ICD-10: A00-R99)
41 for each city, with the data covering part of the period from 1 January 1980 to 31 December 2019, and
42 with varying lengths by location, totalling more than three years. To focus on the impact of heat stress, we

1 used only the warm season data for each city, defined as the location-specific warmest six consecutive
2 months, as listed in Table S2.

3 **Global climate reanalysis data.** We utilize the ERA5 reanalysis data from the European Centre for
4 Medium-Range Weather Forecasts – (ECMWF)³⁵, which integrates multi-source observations and model
5 forecasts, to calculate the HSIs. The hourly 2-m air temperature, 2-m dewpoint temperature, 10-m wind
6 speed, surface pressure, surface downward solar radiation, and precipitation are used, covering 1980-2019.
7 The climate conditions for each city are represented by the reanalysis grid cell (~31 km) that contains the
8 city's geographic coordinates. Prior research has demonstrated the reliability of reanalysis data as a
9 substitute for in-situ data in health impact assessments⁴⁶. Moreover, since meteorological variables other
10 than T_{air} , such as RH, wind speed, and solar radiation are required for the computation of the HSIs,
11 reanalysis data offers a suitable alternative to in-situ measurements in providing consistent historical
12 spatiotemporal coverage required for our analyses.

13 **Heat stress indicators (HSIs).** This study examines eight commonly used HSIs: wet bulb temperature
14 (T_w)²¹, wet bulb globe temperature (T_{WBG})²², simplified wet bulb globe temperature (T_{sWBG})³⁶, heat index
15 (HI)²³, Humidex (H_x)³⁷, apparent temperature (APT)²⁴, lethal heat stress temperature (T_s)¹⁸, and Universal
16 Thermal Climate Index (UTCI)³⁸. The hourly values of each HSI are calculated using ERA5 reanalysis
17 data, and the daily mean and maximum values are assembled by averaging or taking the maximum of the
18 hourly values, taking care to convert to the location-specific time zone. The study analyses all eight
19 indicators for the 739 MCC cities, while T_{WBG} and T_s are excluded from the global land surface grid
20 calculation and the HSIs discrepancy analysis due to computational costs. For further information and the
21 input variables of each HSI, see Table S3. A recent systematic review article provides comprehensive
22 information about these HSIs¹⁴.

23 **The heat-mortality analysis.** We employed distributed lag non-linear models (DLNMs), a well-
24 established method to examine the heat-mortality relationship during the warm season in each city⁵¹.
25 DLNMs are capable of handling complex nonlinear and lagged dependencies often found in heat-mortality
26 studies. We analysed the association between daily mortality and daily max/mean values of each of the
27 eight HSIs (as well as T_{air}) separately using quasi-Poisson regression, for which a quasi-likelihood was
28 used to scale the standard error of the coefficients proportionally to the possible overdispersion⁵¹. The
29 daily mortality and HSIs/ T_{air} series are synchronized based on the local time of each city.

30 In DLNMs, the bi-dimensional exposure-lag-response association is modelled through a combination of
31 two functions defined within a cross-basis term. Specifically, the exposure-response curve is modelled by
32 a natural cubic spline function with two internal knots at the 50th and 90th percentile of the warm season
33 indicator distribution, and the lag-response curve is modelled by a natural spline function with two internal
34 knots at equally spaced values in the log scale over a 10-day lag. As the daily mortality time series is likely
35 to have seasonality and long-term trends independent of temperature, it is necessary to control these
36 patterns in the model so that the short-term association between heat stress and mortality can be detected.
37 We use a natural spline function with 4 degrees of freedom of day of the year to model the seasonality,
38 and a natural spline function of time with one knot/10 years to model the long-term trends of the mortality.
39 This has the same effect as detrending a priori⁵² since the association with temperature (and other HSIs)
40 that is captured is conditional on this trend. The model also includes an indicator to model the intra-week
41 variation of the mortality. The model parameters were based on relevant studies from the MCC
42 Collaborative Research Network^{7,53}. The obtained bidimensional set of coefficients at each city was then

1 reduced across the lag dimension into the overall cumulative exposure-response association curve, which
2 represents the heat-mortality association for all ten days.

3 We used the quasi-Akaike information criterion (qAIC)⁴² and quasi-Bayesian information criterion (qBIC)
4 ⁴² to assess the performance of each indicator in predicting mortality at each city, with a lower qAIC or
5 qBIC value indicating a better fit. The indicator with the smallest qAIC or qBIC value was deemed the
6 best-fit indicator (BFI) for each city. We obtained two groups of BFIs based on the daily mean and
7 maximum value of the indicators, respectively.

8 Finally, we quantified the heat-related mortality in each city during the warm season, based on the T_{air} -
9 fitted model and BFI-fitted model, separately. For each city, the number of heat-related deaths is estimated
10 according to the indicator time series, daily baseline mortality, and the heat-mortality association
11 represented in DLNMs. Then, the total number of heat-related deaths in each city is obtained by summing
12 the daily excess deaths when the indicator is higher than the location-specific optimum value, which is
13 obtained in the fitted DLNMs and represents the indicator value with the lowest mortality risk. Lastly,
14 similar to previous studies^{7,46}, the attributable fraction (AF) of mortality related to heat stress is calculated
15 by dividing the heat-related mortality by the total number of warm season deaths for the same period in
16 each city. We assessed the uncertainty of our estimates by conducting Monte Carlo simulations to generate
17 1,000 samples of the coefficients, which represent the association. We assumed a multivariate normal
18 distribution for the estimated spline model coefficient. From these simulations, we derived empirical
19 confidence intervals (CIs) corresponding to the 2.5th and 97.5th percentiles of the empirical distribution
20 of heat-related mortality.

21 **The supervised machine learning analysis.** To investigate under what conditions city-level mortality
22 shows a stronger association with humid heat, than dry heat (T_{air}), we used a random forest algorithm⁵⁴
23 to analyse multiple features of selected cities and their BFIs. We chose two groups of cities based on the
24 sensitivity of their BFI to RH (Fig. S1). The first group, humid heat-dominant cities, includes cities whose
25 BFI is one of T_w , T_s , T_{WBG} , and T_{sWBG} . The second group, dry heat-dominant cities, includes cities with
26 T_{air} as their BFI. The numbers of humid heat and dry heat-dominant cities are 231 and 222, respectively.

27 We used 13 features related to climatologic, geographic, and socio-economic factors of the selected cities
28 as input (Table S5). The specific values of these features are provided in Table S6. The elevation and
29 distance to the nearest coastline of the city are obtained by matching the city's coordinates to the available
30 open-source data^{55,56}. We used the dominant heat type (dry or humid) of the city as the output of the
31 classification model. The random forest algorithm has been fine-tuned to optimize its performance. The
32 resulting optimized parameters are as follows: the number of trees is set to 500, the number of predictors
33 sampled for splitting at each node is set to 4, and the minimum size of terminal nodes is set to 7. To
34 account for model uncertainty, we ran the random forest algorithm 500 times, using 70% of the data for
35 training and 30% of the data for testing in each run. We report the classification results in a confusion
36 matrix format in Table S7 in the supplementary, which is the summary of all 500 implementations for the
37 testing datasets. On average, the model has an accuracy of 65.6%, precision of 66.3%, and recall of 65.5%,
38 demonstrating its ability to classify the dominant heat type of a city. Substituting RH with specific
39 humidity (Q) in the input features, we obtained comparable classification results with accuracy, precision,
40 and recall of 65.9%, 66.7%, and 65.2%, respectively.

41 Furthermore, the random forest algorithm provides feature importance, which ranks the input features
42 based on their importance in predicting the output. We analysed the importance of the 13 input features in

1 influencing the dominant heat type of a city. The feature importance is calculated based on the decrease
2 in Gini impurity.

4 **Acknowledgments**

5 Q.G., M.H., and T.O. were supported by the Environment Research and Technology Development Fund
6 (JPMEERF23S21120) of the Environmental Restoration and Conservation Agency provided by the
7 Ministry of the Environment of Japan. Q.G. was supported by the Musha Shugyo international travel
8 grants from the School of Engineering, The University of Tokyo. T.O. was supported by the Japan Society
9 for the Promotion of Science (KAKENHI), Grant Number 21H05002. M.N.M. was supported by the
10 European Commission (H2020-MSCA-IF-2020) under REA grant agreement no. 101022870. A.G. was
11 supported by the Medical Research Council-UK (Grant ID: MR/V034162/1) and European Union's
12 Horizon 2020 Project Exhaustion (Grant ID: 820655). J.K. was supported by the Czech Science
13 Foundation, project 23-06749S. AMVC acknowledges funding from the Swiss National Science
14 Foundation (TMSGI3_211626). V.H. acknowledges funding from the European Union's Horizon 2020
15 research and innovation program (H2020-MSCA-IF-2020, Grant No.: 101032087). Y.S. was supported
16 by Brain Pool Plus program funded by the Ministry of Science and ICT through the National Research
17 Foundation of Korea (NRF-2021H1D3A2A03097768), and the National Research Foundation of Korea
18 (NRF) grant funded by the Korean government (MSIT) (NRF-2023R1A2C1004754). The authors would
19 like to thank ECMWF that implementing the Copernicus Climate Change Service (C3S) on behalf of the
20 European Union, and developing and publishing the ERA5 data. The authors would like to thank the
21 developer and contributor of elevation (EarthEnv), and Distance to the Nearest Coast (NASA's Ocean
22 Biology Processing Group) datasets.

23
24 Full List of MCC Collaborative Research Network authors:

25 Rosana Abrutzky²⁶, Yuming Guo^{6,27}, Micheline de Sousa Zanotti Stagliorio Coelho²⁸, Paulo Hilario Nascimento
26 Saldiva²⁹, Eric Lavigne^{30,31}, Nicolás Valdés Ortega³², Patricia Matus Correa³², Haidong Kan³³, Samuel Osorio³⁴,
27 Dominic Roye^{35,36}, Ene Indermitte³⁷, Hans Orru³⁷, Jouni J. K. Jaakkola^{38,39}, Niilo Rytö^{38,39}, Mathilde Pascal⁴⁰,
28 Alexandra Schneider²³, Antonis Analitis¹⁶, Alireza Entezari^{6,41}, Fatemeh Mayvaneh⁴², Ariana Zeka⁴³, Patrick
29 Goodman⁴⁴, Francesca de Donato⁴⁵, Paola Michelozzi⁴⁵, Barrak Alahmad⁴⁶, César De la Cruz Valencia⁴⁷, Magali
30 Hurtado Diaz⁴⁷, Ala Overcenco⁴⁸, Caroline Ameling⁴⁹, Danny Houthuijs⁴⁹, Shilpa Rao⁵⁰, Gabriel Carrasco^{51,52},
31 Xerxes Seposo⁵³, Joana Madureira^{54,55,56}, Susana das Neves Pereira da Silva⁵⁷, Iulian-Horia Holobaca⁵⁸, Fiorella
32 Acquotta⁵⁹, Noah Scovronick⁶⁰, Ho Kim⁶¹, Whanhee Lee^{62,63}, Aurelio Tobias^{64,65}, Carmen Íñiguez^{36,66}, Bertil
33 Forsberg⁶⁷, Martina S. Ragetli^{68,69}, Shih-Chun Pan⁷⁰, Yue Leon Guo^{70,71,72}, Shanshan Li^{6,27}, Rochelle
34 Schneider^{13,73,74}, Valentina Colistro⁷⁵, Antonella Zanobetti⁴⁶, Joel Schwartz⁴⁶, Do Van Dung⁷⁶, Tran Ngoc
35 Dang^{76,77}, Yasushi Honda⁷⁸

36 ²⁶ Universidad de Buenos Aires, Facultad de Ciencias Sociales, Instituto de Investigaciones Gino Germani

37 ²⁷ Department of Epidemiology and Preventive Medicine, School of Public Health and Preventive Medicine, Monash
38 University, Melbourne, Australia

39 ²⁸ Department of Pathology, Faculty of Medicine, University of São Paulo, São Paulo, Brazil

40 ²⁹ INSPER, São Paulo, Brazil

41 ³⁰ School of Epidemiology & Public Health, Faculty of Medicine, University of Ottawa, Ottawa, Canada

42 ³¹ Air Health Science Division, Health Canada, Ottawa, Canada

43 ³² Department of Public Health, Universidad de los Andes, Santiago, Chile

44 ³³ Department of Environmental Health, School of Public Health, Fudan University, Shanghai, China

45 ³⁴ Department of Environmental Health, University of São Paulo, São Paulo, Brazil

- 1 ³⁵ Climate Research Foundation (FIC), Madrid, Spain
- 2 ³⁶ Ciberesp, Madrid, Spain
- 3 ³⁷ Department of Family Medicine and Public Health, University of Tartu, Tartu, Estonia
- 4 ³⁸ Center for Environmental and Respiratory Health Research (CERH), University of Oulu, Oulu, Finland
- 5 ³⁹ Medical Research Center Oulu (MRC Oulu), Oulu University Hospital and University of Oulu, Oulu, Finland
- 6 ⁴⁰ Santé Publique France, Department of Environmental Health, French National Public Health Agency, Saint Maurice, France
- 7 ⁴¹ Faculty of Geography and Environmental Sciences, Hakim Sabzevari University, Sabzevar 9617916487 Khorasan Razavi,
- 8 Iran
- 9 ⁴² University of Münster, Institute of Landscape Ecology, Climatology Research Group, Münster, Germany
- 10 ⁴³ Institute for the Environment, Brunel University London, London, UK
- 11 ⁴⁴ Technological University Dublin, Ireland
- 12 ⁴⁵ Department of Epidemiology, Lazio Regional Health Service, Rome, Italy
- 13 ⁴⁶ Department of Environmental Health, Harvard T.H. Chan School of Public Health, Harvard University, Boston, MA, USA
- 14 ⁴⁷ Department of Environmental Health, National Institute of Public Health, Cuernavaca, Morelos, Mexico
- 15 ⁴⁸ National Agency for Public Health of the Ministry of Health, Labour and Social Protection of the Republic of Moldova
- 16 ⁴⁹ National Institute for Public Health and the Environment (RIVM), Centre for Sustainability and Environmental Health,
- 17 Bilthoven, Netherlands
- 18 ⁵⁰ Norwegian institute of Public Health, Oslo, Norway
- 19 ⁵¹ Health Innovation Laboratory, Institute of Tropical Medicine “Alexander von Humboldt”, Universidad Peruana Cayetano
- 20 Heredia, Lima, Peru
- 21 ⁵² Division of Infectious Diseases, Department of Medicine, University of California, San Diego, United States of America
- 22 ⁵³ Department of Hygiene, Graduate School of Medicine, Hokkaido University
- 23 ⁵⁴ Environmental Health Department, National Institute of Health, Rua Alexandre Herculano, 321, 4000-055 Porto, Portugal
- 24 ⁵⁵ EPIUnit - Instituto de Saude Publica, Universidade do Porto, Porto, Portugal
- 25 ⁵⁶ Laboratório para a Investigação Integrativa e Translacional em Saúde Populacional (ITR), Porto, Portugal
- 26 ⁵⁷ Department of Epidemiology, Instituto Nacional de Saúde Dr. Ricardo Jorge, Lisbon, Portugal
- 27 ⁵⁸ Faculty of Geography, Babes-Bolyai University, Cluj-Napoca, Romania
- 28 ⁵⁹ Department of Earth Sciences, University of Torino, Italy
- 29 ⁶⁰ Department of Environmental Health. Rollins School of Public Health, Emory University, Atlanta, USA
- 30 ⁶¹ Graduate School of Public Health, Seoul National University, Seoul, South Korea
- 31 ⁶² School of Biomedical Convergence Engineering, College of Information and Biomedical Engineering, Pusan National
- 32 University, Yangsan, South Korea
- 33 ⁶³ Institute of Ewha-SCL for Environmental Health (IESEH), College of Medicine, Ewha Womans University, Seoul, Republic
- 34 of Korea
- 35 ⁶⁴ Institute of Environmental Assessment and Water Research (IDAEA), Spanish Council for Scientific Research (CSIC),
- 36 Barcelona, Spain
- 37 ⁶⁵ School of Tropical Medicine and Global Health, Nagasaki University, Nagasaki, Japan
- 38 ⁶⁶ Department of Statistics and Computational Research. Universitat de València, València, Spain
- 39 ⁶⁷ Department of Public Health and Clinical Medicine, Umeå University, Sweden
- 40 ⁶⁸ Swiss Tropical and Public Health Institute, Basel, Switzerland
- 41 ⁶⁹ University of Basel, Basel, Switzerland
- 42 ⁷⁰ National Institute of Environmental Health Science, National Health Research Institutes, Zhunan, Taiwan
- 43 ⁷¹ Environmental and Occupational Medicine, National Taiwan University (NTU) College of Medicine and NTU Hospital,
- 44 Taipei, Taiwan
- 45 ⁷² Graduate Institute of Environmental and Occupational Health Sciences, NTU College of Public Health, Taipei, Taiwan
- 46 ⁷³ European Space Agency (ESA), Φ-lab, Frascati, Italy
- 47 ⁷⁴ Forecast Department, European Centre for Medium-Range Weather Forecast (ECMWF), Reading, UK
- 48 ⁷⁵ Department of Preventive and Social Medicine, School of Medicine, University of the Republic, Montevideo, Uruguay
- 49 ⁷⁶ Department of Environmental Health, Faculty of Public Health, University of Medicine and Pharmacy at Ho Chi Minh City,
- 50 Ho Chi Minh City, Vietnam
- 51 ⁷⁷ Institute of Research and Development, Duy Tan University, Da Nang, Vietnam
- 52 ⁷⁸ Center for Climate Change Adaptation, National Institute for Environmental Studies, Tsukuba, Japan

53
54
55

1 References

- 2 1 Rogers, C. D. W. *et al.* Recent Increases in Exposure to Extreme Humid - Heat Events Disproportionately Affect
3 Populated Regions. *Geophysical Research Letters* **48**, doi:10.1029/2021gl094183 (2021).
- 4 2 Domeisen, D. I. V. *et al.* Prediction and projection of heatwaves. *Nature Reviews Earth & Environment*,
5 doi:10.1038/s43017-022-00371-z (2022).
- 6 3 Li, J., Chen, Y. D., Gan, T. Y. & Lau, N.-C. Elevated increases in human-perceived temperature under climate
7 warming. *Nature Climate Change* **8**, 43-47, doi:10.1038/s41558-017-0036-2 (2018).
- 8 4 Speizer, S., Raymond, C., Ivanovich, C. & Horton, R. M. Concentrated and Intensifying Humid Heat Extremes in the
9 IPCC AR6 Regions. *Geophysical Research Letters* **49**, doi:10.1029/2021gl097261 (2022).
- 10 5 Witze, A. Extreme heatwaves: surprising lessons from the record warmth. *Nature* **608**, 464-465, doi:10.1038/d41586-
11 022-02114-y (2022).
- 12 6 Gasparrini, A. *et al.* Mortality risk attributable to high and low ambient temperature: a multicountry observational
13 study. *Lancet* **386**, 369-375, doi:10.1016/S0140-6736(14)62114-0 (2015).
- 14 7 Vicedo-Cabrera, A. M. *et al.* The burden of heat-related mortality attributable to recent human-induced climate
15 change. *Nat Clim Chang* **11**, 492-500, doi:10.1038/s41558-021-01058-x (2021).
- 16 8 Mora, C. *et al.* Global risk of deadly heat. *Nature Climate Change* **7**, 501-506, doi:10.1038/nclimate3322 (2017).
- 17 9 WMO. Atlas of Mortality and Economic Losses from Weather, Climate and Water Extremes (1970–2012). Report
18 No. 978-92-63-11123-4, (World Meteorological Organization, Geneva, Switzerland, 2014).
- 19 10 Ballester, J. *et al.* The effect of temporal data aggregation to assess the impact of changing temperatures in Europe: an
20 epidemiological modelling study. *Lancet Reg Health Eur* **36**, 100779, doi:10.1016/j.lanepe.2023.100779 (2024).
- 21 11 Ebi, K. L. *et al.* Hot weather and heat extremes: health risks. *Lancet* **398**, 698-708, doi:10.1016/S0140-6736(21)01208-
22 3 (2021).
- 23 12 Sherwood, S. C. How Important Is Humidity in Heat Stress? *Journal of Geophysical Research: Atmospheres* **123**,
24 doi:10.1029/2018jd028969 (2018).
- 25 13 Chakraborty, T., Venter, Z. S., Qian, Y. & Lee, X. Lower Urban Humidity Moderates Outdoor Heat Stress. *AGU*
26 *Advances* **3**, doi:10.1029/2022av000729 (2022).
- 27 14 de Freitas, C. R. & Grigorieva, E. A. A comparison and appraisal of a comprehensive range of human thermal climate
28 indices. *Int J Biometeorol* **61**, 487-512, doi:10.1007/s00484-016-1228-6 (2017).
- 29 15 Kang, S. & Eltahir, E. A. B. North China Plain threatened by deadly heatwaves due to climate change and irrigation.
30 *Nat Commun* **9**, 2894, doi:10.1038/s41467-018-05252-y (2018).
- 31 16 Mishra, V. *et al.* Moist heat stress extremes in India enhanced by irrigation. *Nature Geoscience* **13**, 722-728,
32 doi:10.1038/s41561-020-00650-8 (2020).
- 33 17 Guo, Q., Zhou, X., Satoh, Y. & Oki, T. Irrigated cropland expansion exacerbates the urban moist heat stress in northern
34 India. *Environmental Research Letters* **17**, doi:10.1088/1748-9326/ac64b6 (2022).
- 35 18 Wouters, H. *et al.* Soil drought can mitigate deadly heat stress thanks to a reduction of air humidity. *Sci Adv* **8**,
36 doi:10.1126/sciadv.abe6653 (2022).
- 37 19 Cvijanovic, I., Mistry, M. N., Begg, J. D., Gasparrin, A. & Rodo, X. Importance of humidity for characterization and
38 communication of dangerous heatwave conditions. *NPJ Clim Atmos Sci* **6**, doi:10.1038/s41612-023-00346-x (2023).
- 39 20 Zhang, K. *et al.* Increased heat risk in wet climate induced by urban humid heat. *Nature* **617**, 738-742,
40 doi:10.1038/s41586-023-05911-1 (2023).
- 41 21 Stull, R. Wet-Bulb Temperature from Relative Humidity and Air Temperature. *Journal of Applied Meteorology and*
42 *Climatology* **50**, 2267-2269, doi:10.1175/jamc-d-11-0143.1 (2011).
- 43 22 Liljegren, J. C., Carhart, R. A., Lawday, P., Tschopp, S. & Sharp, R. Modeling the wet bulb globe temperature using
44 standard meteorological measurements. *J Occup Environ Hyg* **5**, 645-655, doi:10.1080/15459620802310770 (2008).
- 45 23 Rothfus, L. P. The heat index equation. (NWS Southern Region Headquarters, Fort Worth, TX, 1990).
- 46 24 ABM. Australian Bureau of Meteorology: About the WBGT and Apparent Temperature indices—Australian Bureau of
47 Meteorology, <http://www.bom.gov.au/info/thermal_stress/#apparent> (2022).
- 48 25 Vecellio, D. J., Wolf, S. T., Cottle, R. M. & Kenney, W. L. Evaluating the 35 degrees C wet-bulb temperature
49 adaptability threshold for young, healthy subjects (PSU HEAT Project). *J Appl Physiol (1985)* **132**, 340-345,
50 doi:10.1152/jappphysiol.00738.2021 (2022).
- 51 26 Armstrong, B. *et al.* The Role of Humidity in Associations of High Temperature with Mortality: A Multicountry,
52 Multicity Study. *Environ Health Perspect* **127**, 97007, doi:10.1289/EHP5430 (2019).
- 53 27 Rodopoulou, S. *et al.* Searching for the best modeling specification for assessing the effects of temperature and
54 humidity on health: a time series analysis in three European cities. *Int J Biometeorol* **59**, 1585-1596,
55 doi:10.1007/s00484-015-0965-2 (2015).

- 1 28 Barnett, A. G., Tong, S. & Clements, A. C. What measure of temperature is the best predictor of mortality? *Environ*
2 *Res* **110**, 604-611, doi:10.1016/j.envres.2010.05.006 (2010).
- 3 29 Vaneckova, P. *et al.* Do Biometeorological Indices Improve Modeling Outcomes of Heat-Related Mortality? *Journal*
4 *of Applied Meteorology and Climatology* **50**, 1165-1176, doi:10.1175/2011jamc2632.1 (2011).
- 5 30 Urban, A. *et al.* Evaluation of the ERA5 reanalysis-based Universal Thermal Climate Index on mortality data in
6 Europe. *Environ Res* **198**, 111227, doi:10.1016/j.envres.2021.111227 (2021).
- 7 31 Zhang, K., Li, Y., Schwartz, J. D. & O'Neill, M. S. What weather variables are important in predicting heat-related
8 mortality? A new application of statistical learning methods. *Environ Res* **132**, 350-359,
9 doi:10.1016/j.envres.2014.04.004 (2014).
- 10 32 Eunice Lo, Y. T. *et al.* Optimal heat stress metric for modelling heat-related mortality varies from country to country.
11 *Int J Climatol* **43**, 5553-5568, doi:10.1002/joc.8160 (2023).
- 12 33 Guo, Y. *et al.* Quantifying excess deaths related to heatwaves under climate change scenarios: A multicountry time
13 series modelling study. *PLoS Med* **15**, e1002629, doi:10.1371/journal.pmed.1002629 (2018).
- 14 34 Baldwin, J. W. *et al.* Humidity's Role in Heat-Related Health Outcomes: A Heated Debate. *Environ Health Perspect*
15 **131**, 55001, doi:10.1289/EHP11807 (2023).
- 16 35 Hersbach, H., Bell, B., Berrisford, P., Biavati, G., Horányi, A., Muñoz Sabater, J., Nicolas, J., Peubey, C., Radu, R.,
17 Rozum, I., Schepers, D., Simmons, A., Soci, C., Dee, D., Thépaut, J-N. ERA5 hourly data on single levels from 1940
18 to present. *Copernicus Climate Change Service (C3S) Climate Data Store (CDS)*, doi:10.24381/cds.adbb2d47 (2023).
- 19 36 Grundstein, A. & Cooper, E. Assessment of the Australian Bureau of Meteorology wet bulb globe temperature model
20 using weather station data. *Int J Biometeorol* **62**, 2205-2213, doi:10.1007/s00484-018-1624-1 (2018).
- 21 37 Masterson J, R. F. *Humidex, A Method of Quantifying Human Discomfort Due to Excessive Heat and Humidity*.
22 (Downsview, Ontario: Environment Canada, Atmospheric Environment, 1979).
- 23 38 Brode, P. *et al.* Deriving the operational procedure for the Universal Thermal Climate Index (UTCI). *Int J Biometeorol*
24 **56**, 481-494, doi:10.1007/s00484-011-0454-1 (2012).
- 25 39 Thiery, W. *et al.* Warming of hot extremes alleviated by expanding irrigation. *Nat Commun* **11**, 290,
26 doi:10.1038/s41467-019-14075-4 (2020).
- 27 40 Byrne, M. P. & O'Gorman, P. A. Understanding Decreases in Land Relative Humidity with Global Warming:
28 Conceptual Model and GCM Simulations. *J Climate* **29**, 9045-9061, doi:10.1175/jcli-d-16-0351.1 (2016).
- 29 41 Byrne, M. P. & O'Gorman, P. A. Trends in continental temperature and humidity directly linked to ocean warming.
30 *Proc Natl Acad Sci US A* **115**, 4863-4868, doi:10.1073/pnas.1722312115 (2018).
- 31 42 Gasparrini, A., Armstrong, B. & Kenward, M. G. Distributed lag non-linear models. *Stat Med* **29**, 2224-2234,
32 doi:10.1002/sim.3940 (2010).
- 33 43 Burnham, K. P. & Anderson, D. R. *Model Selection and Multimodel Inference: A Practical Information-Theoretic*
34 *Approach*. Second Edition edn, (Springer-Verlag New York, Inc., 2002).
- 35 44 Ahn, Y., Tuholske, C. & Parks, R. M. Comparing Approximated Heat Stress Measures Across the United States.
36 *Geohealth* **8**, e2023GH000923, doi:10.1029/2023GH000923 (2024).
- 37 45 Lee, J. & Dessler, A. E. Improved Surface Urban Heat Impact Assessment Using GOES Satellite Data: A Comparative
38 Study With ERA - 5. *Geophysical Research Letters* **51**, doi:10.1029/2023gl107364 (2024).
- 39 46 Mistry, M. N. *et al.* Comparison of weather station and climate reanalysis data for modelling temperature-related
40 mortality. *Sci Rep* **12**, 5178, doi:10.1038/s41598-022-09049-4 (2022).
- 41 47 Guo, Q., Yuan, L., Ng, C. F. S. & Hashizume, M. Evaluating Japan's revised heat-health warning system in the face
42 of recent escalating heat stress. *Environmental Research Letters* **19**, doi:10.1088/1748-9326/ad3a81 (2024).
- 43 48 He, C. *et al.* The overlooked health impacts of extreme rainfall exposure in 30 East Asian cities. *Nature Sustainability*
44 **7**, 423-431, doi:10.1038/s41893-024-01294-x (2024).
- 45 49 Huang, W. T. K. *et al.* Economic valuation of temperature-related mortality attributed to urban heat islands in
46 European cities. *Nat Commun* **14**, 7438, doi:10.1038/s41467-023-43135-z (2023).
- 47 50 Im, E. S., Pal, J. S. & Eltahir, E. A. B. Deadly heat waves projected in the densely populated agricultural regions of
48 South Asia. *Sci Adv* **3**, e1603322, doi:10.1126/sciadv.1603322 (2017).
- 49 51 Gasparrini, A. Modeling exposure-lag-response associations with distributed lag non-linear models. *Stat Med* **33**, 881-
50 899, doi:10.1002/sim.5963 (2014).
- 51 52 Franzke, C. L. E. Nonlinear climate change. *Nature Climate Change* **4**, 423-424, doi:10.1038/nclimate2245 (2014).
- 52 53 Vicedo-Cabrera, A. M., Sera, F. & Gasparrini, A. Hands-on Tutorial on a Modeling Framework for Projections of
53 Climate Change Impacts on Health. *Epidemiology* **30**, 321-329, doi:10.1097/EDE.0000000000000982 (2019).
- 54 54 Breiman, L. Random Forests. *Machine Learning* **45**, 5-32, doi:10.1023/a:1010933404324 (2001).
- 55 55 Amatulli, G. *et al.* A suite of global, cross-scale topographic variables for environmental and biodiversity modeling.
56 *Sci Data* **5**, 180040, doi:10.1038/sdata.2018.40 (2018).
- 57 56 Stumpf, R. Distance to the Nearest Coast. *NASA's Ocean Biology Processing Group* (2009).

1 Data and materials availability

2 The ERA5 data are freely available from the Climate Data Store
 3 (<https://cds.climate.copernicus.eu/cdsapp#!/home>). The elevation data and distance to the nearest
 4 coastline data can be obtained from EarthEnv (<https://www.earthenv.org/topography>) and ERDDAP
 5 (https://pae-paha.pacioos.hawaii.edu/erddap/griddap/dist2coast_1deg_land.html), respectively. The
 6 mortality data have been obtained through a restricted data use agreement with each national institute and
 7 are therefore not available for public dissemination (<https://mccstudy.lshhtm.ac.uk/>), and the intermediary
 8 data obtained from the heat-mortality association analysis is provided at https://github.com/superqiang-g-cc/RH_Role_Mortality. All calculations and analyses were conducted using Python (version 3.7.12) and
 9 R (version 4.0.3). All figures were produced using the freely available visualization libraries in Python
 10 3.7.12 (such as Matplotlib). The relevant portions of the computer code used to process the results and
 11 develop the figures are available at https://github.com/superqiang-g-cc/RH_Role_Mortality.
 12

14 Figures and Tables

16 **Fig. 1 | Long-term trends of the extremes of 6 heat stress indicators (HSIs).** **a-c**, The linear trends (per
 17 decade) of the of $T_{\text{air } X_{99}}$ (99th percentile of the annual values of each year) (**a**), and specific humidity (Q)
 18 (**b**) and relative humidity (RH) (**c**) of the high-temperature days (daily $T_{\text{air}} > T_{\text{air } X_{99}}$) between 1980-2019.
 19 The results of **a-c** are based on the daily mean value. Stippling denotes the linear trend reaches the
 20 significant level ($p < 0.05$). **d,e**, The sum of the HSI vote of T_w , T_{swBG} , H_x , APT, UTCI, and HI. The HSI vote is
 21 set as 1 when HSI X_{99} shows a positive trend between 1980-2019 and is set as -1 when negative. Results
 22 based both on the daily mean (**d**) and daily maximum (**e**) values of HSIs are presented. Stippling denotes
 23 the linear trend of at least one HSI reaching the significant level ($p < 0.05$).

25 **Fig. 2 | Intra-annual peak time difference among air temperature (T_{air}) and heat stress indicators (HSIs).**
 26 **a**, Averaged intra-annual peak time (day of year when T_{air} reaches annual peak) of T_{air} for 1980-2019. **b-g**,
 27 Difference between averaged intra-annual peak time of corresponding HSI and T_{air} (the former minus
 28 the latter) for 1980-2019. **h-k**, Occurrence frequency of the hottest 10 days measured by T_{air} and 8 HSIs
 29 for 4 cities: Austin (**h**), Brasilia (**i**), London (**j**), and Bangkok (**k**) for 1980-2019. The occurrence frequency
 30 is obtained by Gaussian kernel density estimation.

32 **Fig. 3 | The best-fit indicator (including air temperature (T_{air}) and heat stress indicators (HSIs)) in
 33 modelling/predicting daily human mortality for 739 MCC cities.** **a**, The indicator with the minimum qAIC
 34 when fitting to the human mortality (defined as best-fit indicator, BFI). The colour of the BFI is presented
 35 based on their sensitivity to the humidity (Fig. S1, e.g., T_{air} (zero sensitivity to humidity), T_w (maximum
 36 sensitivity to humidity)). The number in the bracket represents the rank in the sensitivity to humidity of
 37 the HSI. **b**, The number of cities and their locations under each BFI group. The results are based on the
 38 daily mean value of the indicators.

1 **Fig. 4 | The factors that influence the lethal heat stress type (dry or humid) for city-level human**
2 **mortality. a**, The feature importance of 13 input features (Table S5) for the random forest algorithm
3 classifying lethal heat stress type. The thick black line indicates the uncertainty in 500 times
4 implementations. **b**, The Spearman correlation coefficient between daily mean air temperature and
5 relative humidity (C_{T-RH}) for 739 MCC cities. **c**, The distribution of the C_{T-RH} for cities versus their best-fit
6 indicators (BFIs) for predicting mortality. The distribution density is obtained by Gaussian kernel density
7 estimation.

8

9 **Fig. 5 | The seasonality of relative risk (RR) of heat stress for 4 cities (Miami, Bristol, Ho Chi Minh City,**
10 **and Taipei). a, c, e, g**, Exposure-response associations estimated by air temperature (T_{air} , black) and best-
11 fit indicator (BFI, red) (with 95% confidence interval, shaded area). The numbers indicate the optimum
12 of T_{air} and BFI with the lowest $RR = 1$, and the vertical dotted lines indicate the 95th percentile of local-
13 specific warm-season indicator value. **b, d, f, h**, The averaged intra-annual variation of RR estimated by
14 T_{air} (black) and BFI (red) during the warm season. The line represents the RR time series, and the shaded
15 area represents the days under heat stress (indicator value > optimum). The numbers indicate the
16 attributable fraction (AF) of death related to heat and the corresponding 95% confidence interval (CI).
17 The intra-annual time series is the averaged results of 1980-2019.

18

19

ACCEPTED MANUSCRIPT

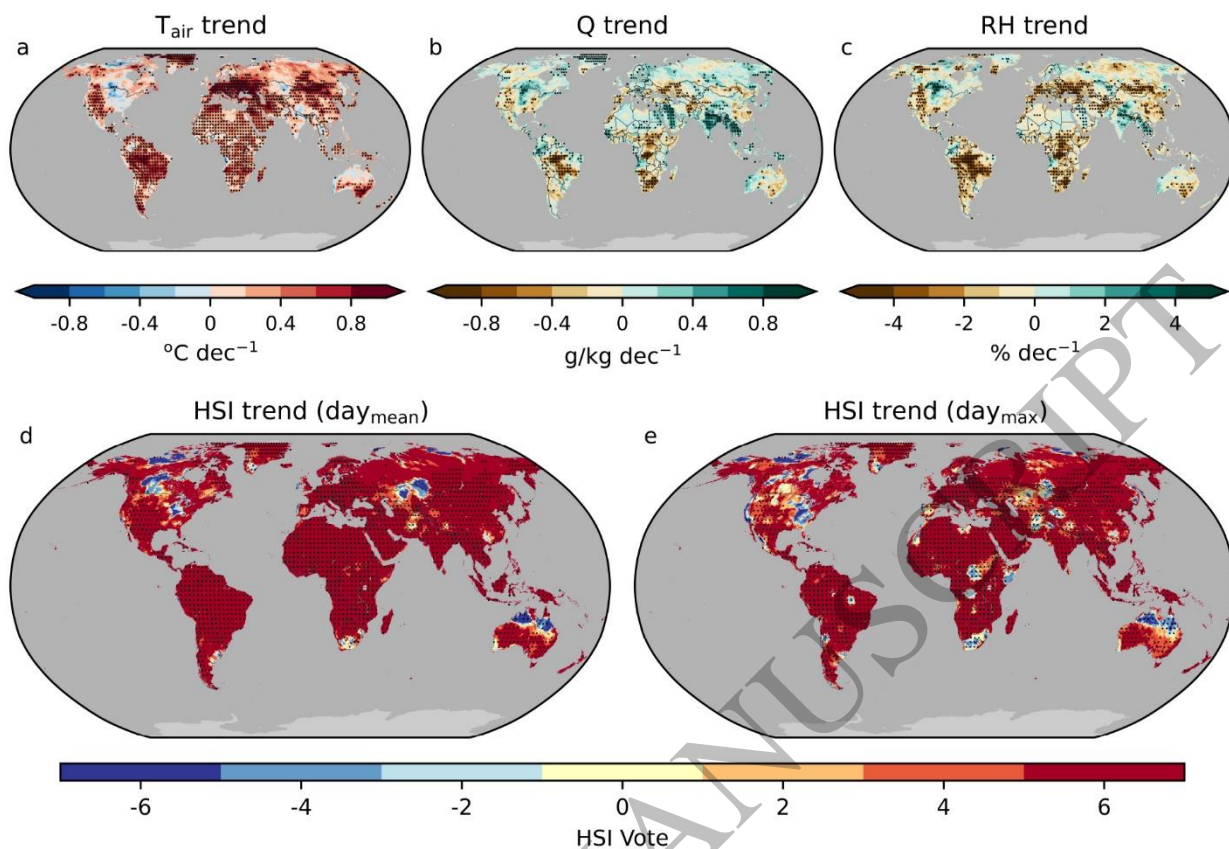


Figure 1
165x112 mm (x DPI)

1
2
3
4

ACCEPTED MANUSCRIPT

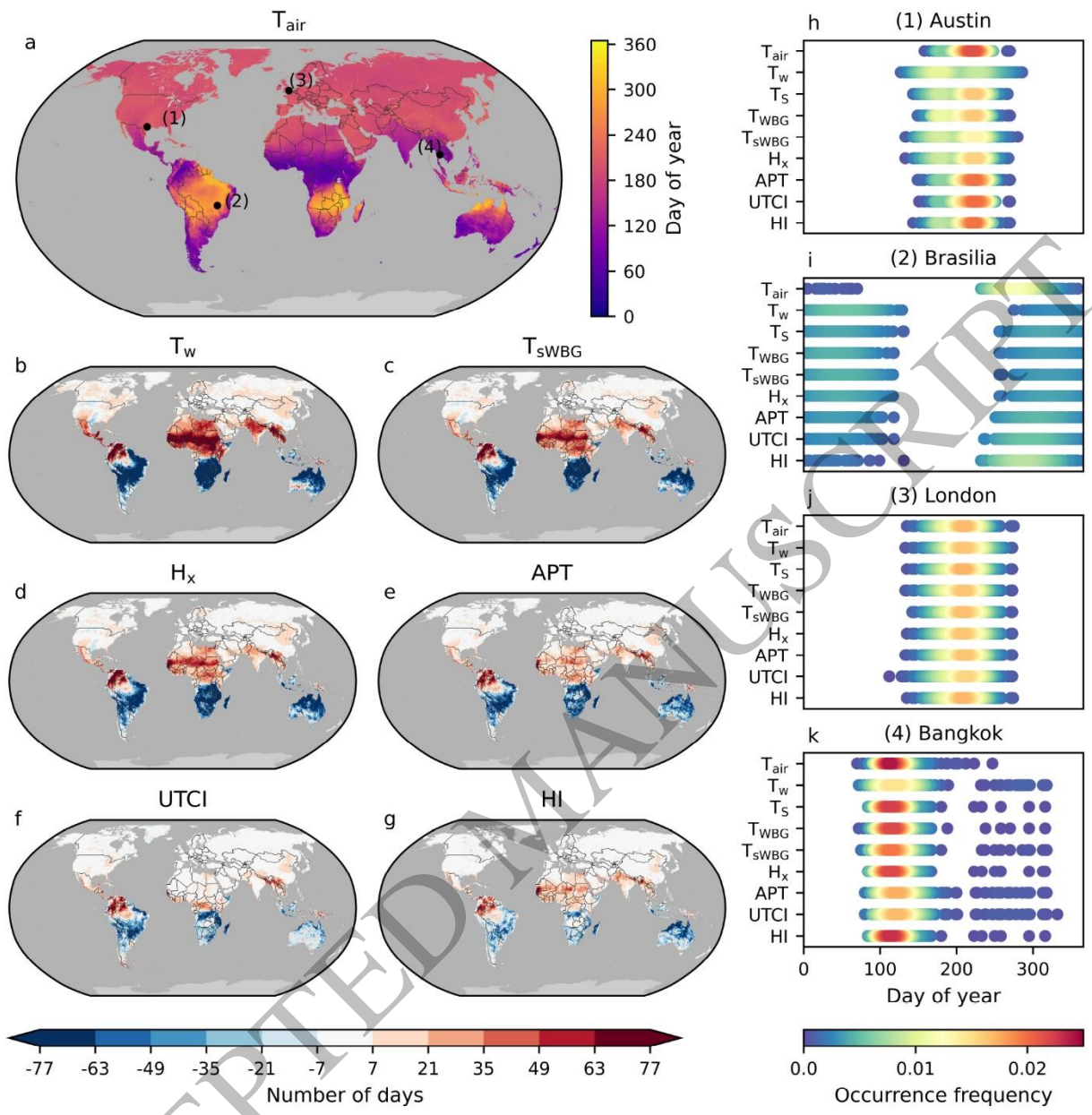


Figure 2
165x163 mm (x DPI)

1
2
3
4

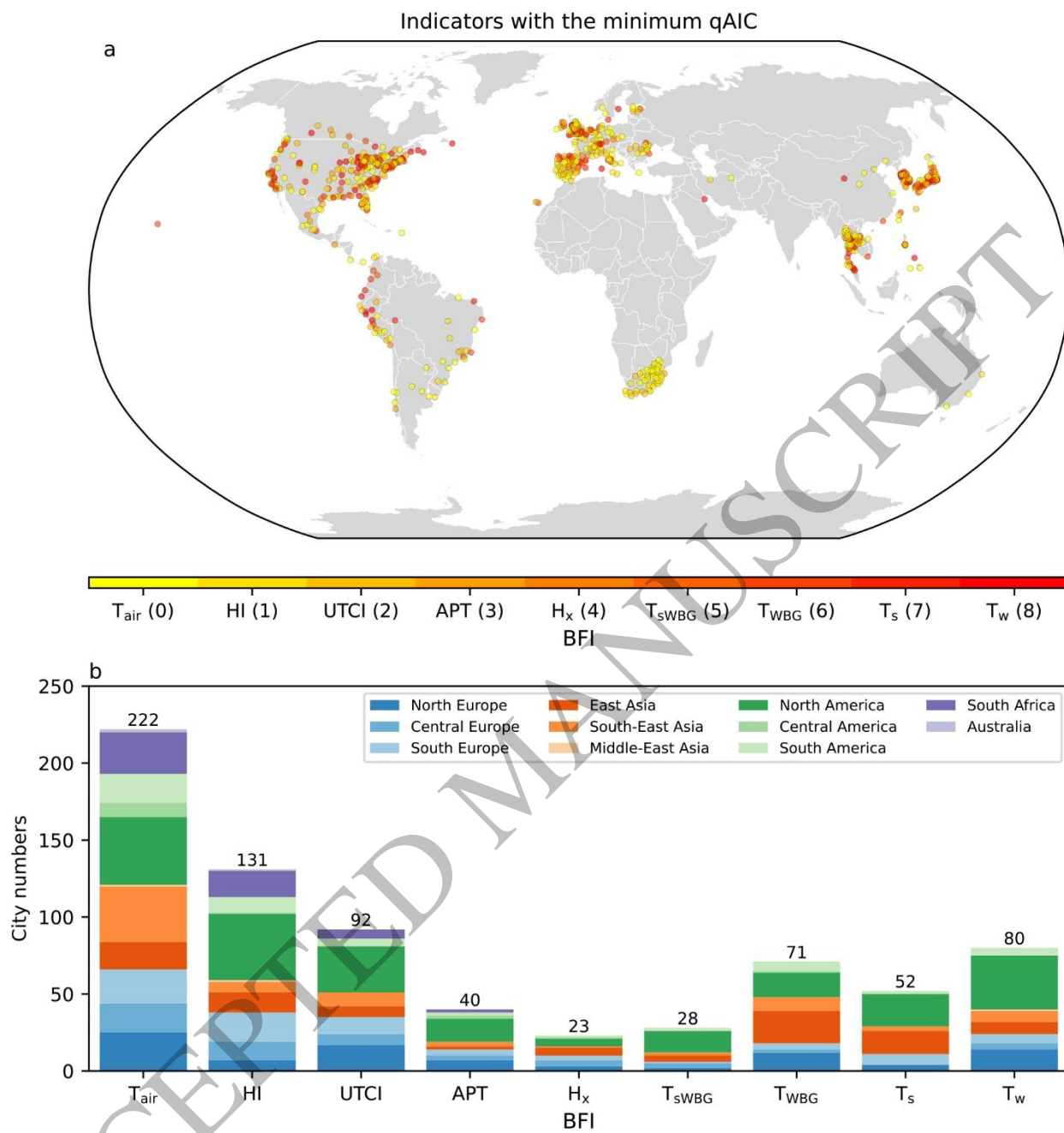


Figure 3
165x175 mm (x DPI)

1
2
3
4

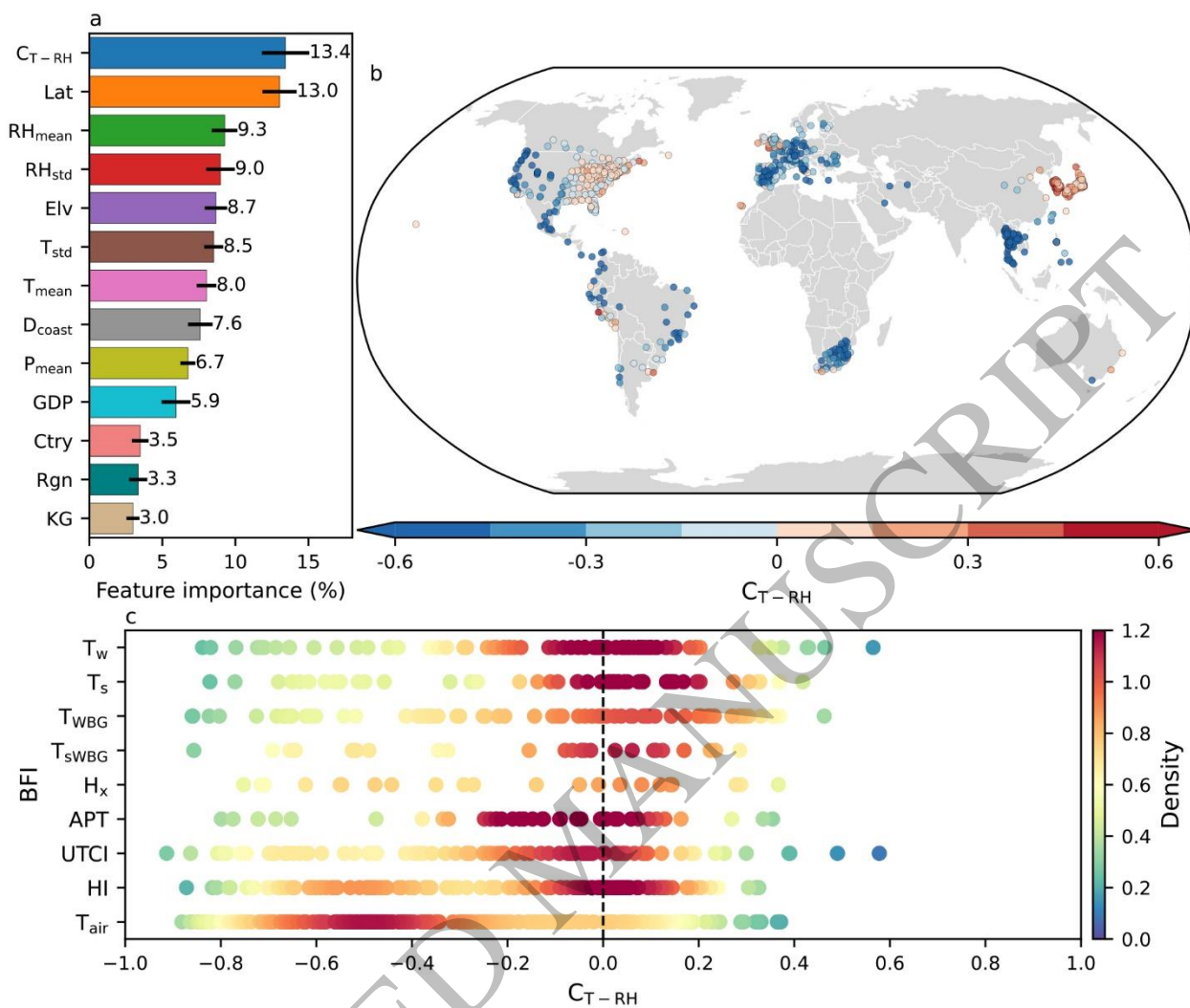


Figure 4
165x142 mm (x DPI)

1
2
3
4

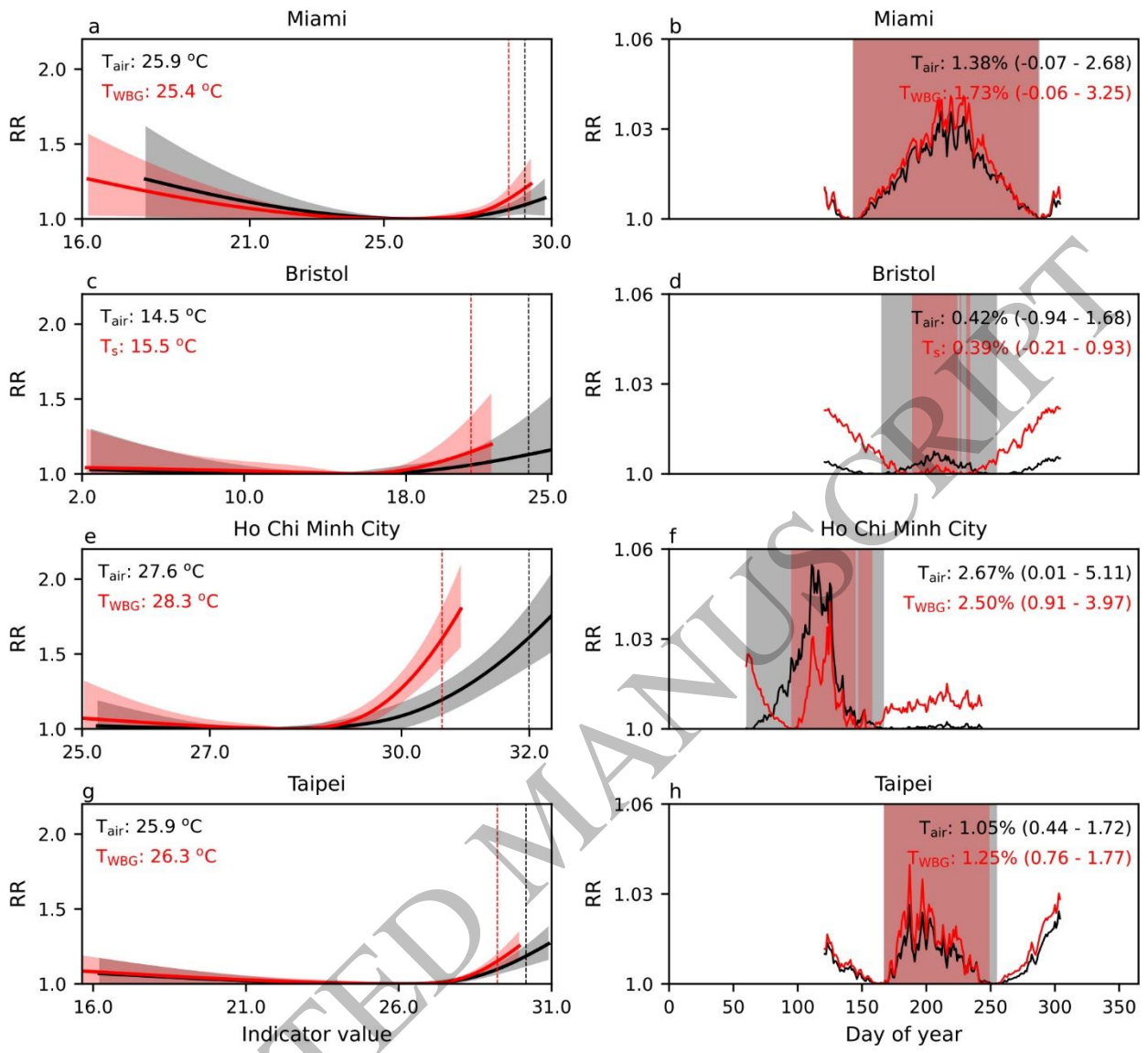


Figure 5
165x152 mm (x DPI)

1
2
3